

# STATUS OF THE CONTINUOUS GRAVITATIONAL WAVE SEARCHES IN THE ADVANCED DETECTOR ERA

M. Bejger (for the LIGO-Virgo Collaboration)

*Nicolaus Copernicus Astronomical Center, Polish Academy of Sciences, ul. Bartycka 18, 00-716, Warszawa, Poland*

Periodic (almost monochromatic) gravitational waves emitted by rotating, asymmetric neutron stars are intriguing potential signals in the sensitivity band of Advanced LIGO and Advanced Virgo detectors. These signals are related to elastic and magnetic stresses in the neutron-star interior, as well as to various possible instabilities, and thus are interesting from the point of view of the largely-unknown neutron star structure. I will describe the main challenges related to these searches, the current state of the data-analysis methods and plans for the future.

## 1 Introduction

Recent first direct detections of gravitational waves with the two LIGO detectors<sup>1,2</sup> create an unprecedented opportunity for studying the Universe through a novel, never before explored channel of spacetime fluctuations. Advanced LIGO<sup>3</sup> and Advanced Virgo<sup>4</sup>, few-kilometer long arm laser interferometric detectors are sensitive in the range of frequencies between 10 Hz and a few kHz. They registers a coherent signal emitted by a bulk movement of large, rapidly-moving masses. Once emitted, gravitational waves are weakly coupled to the surrounding matter and propagate freely without scattering. This has to be contrasted with the electromagnetic emission which originates at the microscopic level, is strongly coupled to the surroundings and often reprocessed; it carries a reliable information from the last scattering surface only. Gravitational wave observations are therefore the perfect counterpart to the electromagnetic observations as they may provide us with information impossible to obtain by other means.

In addition to inspiralling and merging binary systems, among promising sources of gravitational radiation are all asymmetric collapses and explosions e.g., supernovæ, wide binary systems, rotating deformed stars (gravitational-wave ‘pulsars’ of continuous and transient nature), as well as stochastic background waves produced by whole populations of sources.

In the following we will briefly describe astrophysical motivation behind continuous gravitational waves produced by rotating deformed neutron stars (Sect. 2), data-analysis methods and computational challenges related to them (Sect. 3), Advanced LIGO O1 run results (Sect. 4), and plans for the future (Sect. 5).

## 2 Astrophysical motivation

Neutron stars are the most relativistic, dense and compact *material* objects in the Universe. Their compactness i.e., mass-to-radius ratio  $2GM/Rc^2$  reaches 0.5 ( $G$  being the Newton’s constant,  $c$  the speed of light); for comparison, the compactness of the most compact objects, black holes, equals 1. Their average density surpasses the nuclear saturation density i.e., the density

of atomic nuclei. At these densities matter exists most probably in an ‘exotic’ phase, e.g., as de-confined quarks. Neutron stars are self-gravitating objects stabilized by strong force interactions, gigantic nuclei of masses up to  $2 M_{\odot}$ , radii about  $10 - 15$  km with surface magnetic fields of  $10^8 - 10^{15}$  Gauss, that can spin several hundred times per second. Comparison of realistic models of neutron stars with a variety of astrophysical observations - including the gravitational waves they emit - is the only way to peek into a realm of dense matter strong interactions much above the nuclear saturation density.

Neutron stars provide truly unique conditions to study matter at the most extreme densities, pressures, and in the presence of powerful magnetic fields. These conditions cannot be reproduced (or even approximated) in terrestrial laboratories. At present, about 2500 neutron stars are known, and an estimated number of  $10^8 - 10^9$  exists in every galaxy similar to ours. Neutron stars play an important role in many astrophysical phenomena: they are observed in all the EM spectrum as radio-, X- and  $\gamma$ -pulsars, magnetars, are present in supernovæ remnants, in many accreting systems and in relativistic double neutron star binaries, yet very little is known about their internal composition. What is conventionally accepted is that at least some part of neutron-star interior - the outer part about 1 km thick called the crust, corresponding to densities *below* the nuclear saturation density - is in the crystalline state.

In the following we will focus on rotating, non-axisymmetric neutron stars as sources of continuous periodic gravitational wave emission. Continuous gravitational wave is by definition a long-lived phenomenon,  $T > T_{obs}$ , and its frequency  $f_{GW}$  is somehow proportional to the spin frequency of the star  $f$ ,  $f_{GW} \propto f$ . There are several proposed astrophysical mechanisms providing the necessary asymmetry, which in the case of a rotating star is the source of time-varying quadrupole required for the gravitational-wave emission. Mechanisms include neutron-star “mountains”, supported by elastic and/or magnetic stresses ( $f_{GW} = 2f$ ), oscillations (e.g., r-modes<sup>5</sup>,  $f_{GW} = 4/3f$ ), free precession ( $f_{GW} \propto f + f_{prec}$ ) and accretion that drives the deformation from r-modes, thermal gradients and magnetic fields ( $f_{GW} \simeq f$ ). For a recent review see<sup>6</sup>.

The most-commonly used and the simplest model of the non-axisymmetric rotating neutron star radiating purely quadrupolar waves consists of a triaxial ellipsoid (with moments of inertia along the axes  $I_1, I_2, I_3$ ), rotating about one of the principal directions of its moment of inertia tensor ( $I_3$ , say). Such a body radiates GWs at the frequency twice the rotational frequency of the star,  $2\pi f_{GW} = \Omega_{GW} = 2\Omega$ . The strain signal at the detector changes in time as

$$h(t) = h_0 \left( \frac{1}{2} F_+(t, \alpha, \delta, \psi) (1 + \cos^2 \iota) \cos(\phi(t) + \phi_0) + F_\times(t, \alpha, \delta, \psi) \cos \iota \cos(\phi(t) + \phi_0) \right), \quad (1)$$

where  $h_0$  is the gravitational-wave strain amplitude,  $\alpha$  and  $\delta$  are right ascension and declination of the source in the sky,  $\psi$  is the polarization angle, and  $\iota$  the inclination of the rotation axis to the line of sight. Phase of the signal  $\phi(t) + \phi_0$  incorporates the possible evolution of the spin frequency.  $F_+$  and  $F_\times$  are the antenna responses of the detector, corresponding to two gravitational-wave polarizations + and  $\times$ .

From the quadrupole formula<sup>7</sup>, amplitude  $h_0$  is estimated as follows:

$$h_0 = \frac{16\pi^2 G}{c^4} \frac{I \epsilon f^2}{d} = 4 \times 10^{-25} \left( \frac{\epsilon}{10^{-6}} \right) \left( \frac{I}{10^{45} \text{ g cm}^2} \right) \left( \frac{f}{100 \text{ Hz}} \right)^2 \left( \frac{100 \text{ pc}}{d} \right), \quad (2)$$

where  $I \equiv I_3$ ,  $f = \Omega/2\pi$ ,  $\epsilon = (I_1 - I_2)/I$  is the fiducial equatorial ellipticity of the star (a “deformation”), and  $d$  is typical distance in the Galaxy. According to theoretical studies of the dense matter equation of state<sup>8,9,10</sup>, nucleonic matter may sustain deformations up to  $\epsilon \simeq 10^{-6} - 10^{-7}$ , whereas for quark matter  $\epsilon$  can reach  $10^{-4} - 10^{-5}$ .

Observations of the majority of known pulsars show that their spin frequency slowly decreases,  $\dot{f} < 0$  (exceptions are pulsars in binary systems which can be spun-up by the angular momentum transfer from the accretion disk). A useful quantity related to the amount of kinetic

(rotational) energy of the star is the so-called spin-down limit. It is derived by assuming that the gravitational-wave emission alone is responsible for the change in the rotational energy,  $\dot{E}_{\text{rot}}$ . For  $E_{\text{rot}} = 2\pi^2 I f^2$ ,  $\dot{E}_{\text{rot}} \propto I f \dot{f}$  is equated with the GW emission,  $\dot{E}_{\text{GW}} \propto \epsilon^2 I^2 f^6$  to obtain the spin-down limit amplitude

$$h_{\text{sd}} = \frac{1}{d} \sqrt{\frac{5GI}{2c^3} \frac{|\dot{f}|}{f}} = 8 \times 10^{-24} \sqrt{\left(\frac{I}{10^{45} \text{ g cm}^2}\right) \left(\frac{|\dot{f}|}{10^{-10} \text{ Hz/s}}\right) \left(\frac{100 \text{ Hz}}{f}\right) \left(\frac{100 \text{ pc}}{d}\right)}. \quad (3)$$

Comparison with Eq. 2 results in the limiting deformation  $\epsilon_{\text{sd}}$ :

$$\epsilon_{\text{sd}} = 2 \times 10^{-5} \sqrt{\left(\frac{10^{45} \text{ g cm}^2}{I}\right) \left(\frac{100 \text{ Hz}}{f}\right)^5 \left(\frac{|\dot{f}|}{10^{-10} \text{ Hz/s}}\right)} = 0.2 \left(\frac{h_{\text{sd}}}{10^{-24}}\right) f^{-2} I_{45}^{-1} d_{\text{kpc}}. \quad (4)$$

A star with  $\epsilon_{\text{sd}}$  would spin-down solely by gravitational-wave radiation. In reality, the ellipticity is smaller, so the results ‘beating the spin-down limit’ probe the physically interesting range of ellipticities and set the upper limit for the ellipticity given object has. We will come back to the spin-down limit in Sect. 4.

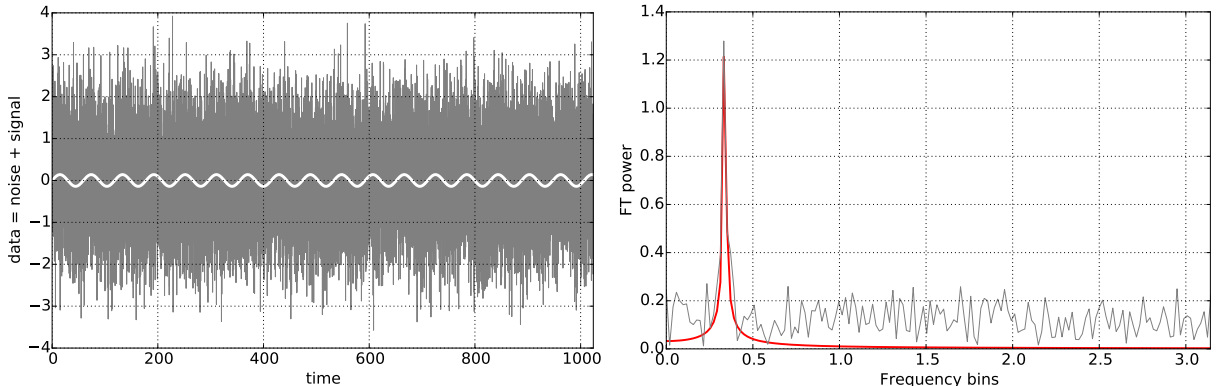


Figure 1 – Periodic signal hidden in white Gaussian noise (left), and the Fourier transform of this time series (right).

### 3 Data-analysis methods and computational challenges

Searching for long-lived, weak gravitational wave signals is a particularly cumbersome task, especially when nothing is known about its parameters. Eq. 2 shows that their strain amplitude is much smaller than e.g., the characteristic strain amplitude of O1 detections,  $h \simeq 10^{-21}$ . Fortunately, one may search for weak signals hidden deeply in the noise provided a waveform of the signal is known. The idea of such a search would be to compute the cross correlation between the data and a parametrised template waveform in order to find parameters of the best match. Techniques of this sort are called the matched filtering methods<sup>11,12,13</sup>. Matched filtering provide an optimal detection statistic (it maximizes the signal-to-noise ratio) if noise is Gaussian.

#### 3.1 Example: signal-to-noise ratio for a periodic signal

An instance of a strictly periodic signal “buried” in the stationary white Gaussian noise is presented in Fig. 1. We will estimate the signal-to-noise ratio  $\rho$  by approximating the output of the matched filter, which in the case of a periodic signal is simply the Fourier transform. The scalar product  $(x|y)$  is defined using the Fourier transform as

$$(x|y) = 4\Re \int_0^\infty \frac{\tilde{x}(f)\tilde{y}^*(f)}{S_n(f)} e^{2\pi i f t} df, \quad (5)$$

where  $*$  denotes complex conjugation,  $\Re$  is the real part of the integral, and  $\tilde{x}(f)$  and  $\tilde{y}(f)$  are the Fourier transform of the time-domain data series:

$$\tilde{x}(f) = \int_{-\infty}^{\infty} x(t) e^{-2\pi i f t} dt, \quad \text{with the inverse transform} \quad x(t) = \int_{-\infty}^{\infty} \tilde{x}(f) e^{2\pi i f t} df. \quad (6)$$

$S_n(f)$  is the one-sided power spectral density of the detector's noise. For a stable detector we may assume the that  $S_n(f) \approx S_0 = \text{const.}$  over the data span. From the Parseval theorem,

$$(x|y) \approx \frac{2}{S_0} \int_0^T x(t) y(t) dt. \quad (7)$$

For the additive noise process, the data  $s(t)$  is defined as the sum of the signal and the noise:  $s(t) = h(t) + n(t)$ . The matched filter output of the data stream  $s(t)$  with a filter template  $h_{\text{templ.}}(t)$  (correlation of the data containing a possible signal with its model) is

$$4\Re \int_0^{\infty} \frac{\tilde{s}(f) \tilde{h}_{\text{templ.}}^*(f)}{S_n(f)} e^{2\pi i f t} df. \quad (8)$$

The optimal signal-to-noise ratio is defined as  $\rho := \sqrt{(h|h)}$ . For a periodic signal  $h(t) = h_0 \cos(\phi(t) + \phi_0)$ , we will assume that the data span  $T_0$  is much longer than the period of the wave,  $P_0 = 1/f_0$ , and that the phase can be expanded in the series  $\phi(t) = \sum_k a_k t^{k+1}$ . Also

$$\frac{1}{T_0} \int_0^{T_0} \cos(n\phi(t)) dt \approx \frac{1}{T_0} \int_0^{T_0} \sin(n\phi(t)) dt \approx 0 \quad (9)$$

for integers  $n > 0$ . Integrating the  $\rho^2$  for  $h(t) = h_0 \cos(\phi(t) + \phi_0)$  gives the estimate for the optimal signal-to-noise ratio for a periodic signal of the amplitude  $h_0$

$$\rho = \left( \frac{2}{S_0} \int_0^{T_0} (h(t))^2 dt \right)^{1/2} \left( \frac{2}{S_0} \int_0^{T_0} h_0^2 \cos^2(\phi(t) + \phi_0) dt \right)^{1/2} \approx h_0 \left( \frac{T_0}{S_0} \right)^{1/2}. \quad (10)$$

It is clear that even for a small  $h_0$  one can reach a satisfactory signal-to-noise ratio with a sufficiently long stretch of data.

In practice, on top of the secular spin-down modulation mentioned before (to describe this feature, one says that the signal is *almost monochromatic*), the signal is modulated by the movement of the detector with respect to the source. Since the Advanced LIGO and Advanced Virgo detectors are placed on Earth, the presence of other planets and Earth's rotation influences signal's amplitude and phase. Demodulation to a frame connected with the Solar System Barycenter (the place in the Solar System that moves the least with respect to the source), precise ephemerides of the movement of planets are used. The fact that the detectors are moving with respect to the source isn't necessary a bad thing, though: detector movement distinguishes a real signal from local spectral artifacts, called the "stationary lines".

### 3.2 Example: the $\mathcal{F}$ -statistic

A conceptually relatively simple method to develop a detection statistic using the time-domain data  $s(t)$  is the  $\mathcal{F}$ -statistic<sup>14</sup>. For a triaxial rotating neutron star model (Eq. 1, the statistic is obtained by maximizing the likelihood ratio function with respect to the four unknown parameters:  $h_0$ ,  $\phi_0$ ,  $\iota$ , and  $\psi$ . This leaves, in case when only first derivative of  $f$  is taken into account, a function of four parameters:  $f$ ,  $\dot{f}$ ,  $\alpha$  and  $\delta$ . These four parameters form a parameter space in which the signal's best match will be searched for. Assuming that the observation time  $T_0$  is the integer multiple of sidereal days, and that the bandwidth is narrow (so that the spectral density of the noise  $S_0$  is constant), the  $\mathcal{F}$ -statistic is evaluated<sup>15</sup> as

$$\mathcal{F} = \frac{2}{S_0 T_0} \left( \frac{|F_a|^2}{\langle a^2 \rangle} + \frac{|F_b|^2}{\langle b^2 \rangle} \right), \quad (11)$$

with

$$F_a = \int_0^{T_0} s(t)a(t) \exp(-i\phi(t))dt, \quad F_b = \dots, \quad \langle a^2 \rangle = \int_0^{T_0} a(t)^2 dt, \quad \langle b^2 \rangle = \dots, \quad (12)$$

$F_a$  and  $F_b$  being the generalizations of the Fourier transforms from the previous section. Amplitude modulation functions  $a(t)$  and  $b(t)$  are related to detector's antenna response ( $F_+ = a(t) \cos 2\psi + b(t) \sin 2\psi$ ,  $F_\times = -a(t) \sin 2\psi + b(t) \cos 2\psi$ ) and depend on the sources' sky position  $\alpha$  and  $\delta$ , and the phase modulation function  $\phi(t)$  depends also on the frequency  $f$  and spin-down of the source,  $\dot{f}$ . The signal-to-noise ratio  $\rho$  is related to  $\mathcal{F}$  as follows:  $\rho = \sqrt{2(\mathcal{F} - 2)}$ .

### 3.3 Taxonomy of search methods

Continuous gravitational-wave searches can be divided according to the amount of information one has about the sources.

The *targeted searches* are most often based on matched filtering (data of length  $T_0$  correlated with signal templates). Position,  $f$  and  $\dot{f}$ , sometimes also the source's orientation are known. In this case the expected strain amplitude scales like  $h_0 \propto \sqrt{S/T_0}$ , where  $S$  is the amplitude spectral density at the expected gravitational-wave frequency.

*Directed searches* cover the intermediate cases when only some parameters are known, e.g., the position of the source. Astrophysically, they may be relevant to supernovae remnants, the Galactic center, globular clusters, accreting neutron stars in binary systems (e.g., the brightest X-ray source in the sky, Sco X-1).

*All-sky searches* are the most demanding types of searches. Source parameters and positions are not known, which makes the parameter space large and the problem becomes very quickly computationally bound. In order to mediate this, hierarchical approaches are being used. Instead of analyzing the whole  $T_0$  data span at once, the data is divided into  $N$  data segments of length  $T_s$ , which are analyzed coherently, and the resulting information is combined incoherently. The expected strain amplitude scales like  $h_0 \propto \sqrt{S/T_s}/N^{1/4}$ . The most sophisticated example of the hierarchical approach is the volunteer-driven Einstein@Home project <sup>a</sup>.

### 3.4 Example: computational cost for an all-sky search

In order to optimally cover the  $(f, \dot{f}, \alpha, \delta)$  parameter space of an all-sky search at all possible frequencies, a grid of parameters is obtained as a solution to the covering problem with constraints (a constraint being e.g., a condition that the optimal  $(\dot{f}, \alpha, \delta)$  lattice coincides with points in  $f$  corresponding to the Fourier frequencies bins of the Fast Fourier Transform algorithm). Typically, the number of points in  $\dot{f}, \alpha, \delta$  scales with some positive power of  $T_0$ , so, depending on the details of the implementation<sup>16</sup>, the computational demand scales like

$$\underbrace{T_0^2}_{\dot{f}} \times \underbrace{T_0^{[0-3]}}_{\alpha, \delta} \times \underbrace{T_0 \log(T_0)}_{f \text{ by FFT}} = T_0^{[3-6]} \log(T_0), \quad (13)$$

which is very prohibitive for large  $T_0$ . A coherent search of  $T_0 \simeq 1 \text{ yr}$  of data (comparable with ongoing and planned Advanced LIGO/Virgo runs) in the broad sensitivity band of the detectors (10 - 2000 Hz) requires *zettaFLOPS* ( $10^{21}$  FLOPS) scale supercomputers. The solution is a hierarchical scheme: divide the data  $T_0$  into a number  $N$  shorter length  $T_s$ ,  $T_s \simeq \text{days}$ , data segments and perform a coherent search in each of them (search in narrow frequency bands of bandwidth  $B$ , Nyquist sampling time  $\delta t = 1/2B$ , number of data points  $N_p = T_s/\delta t = 2T_s B$ ). This is feasible on a typical petaFLOP scale supercomputer (cluster), yet still requires millions of CPU-hours. Second incoherent stage consists of searching for coincidences between different  $T_s$  segments. Surviving outliers present in sufficiently many segments (candidate signals with

---

<sup>a</sup><https://einsteinathome.org>

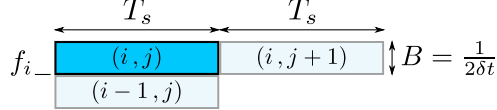


Figure 2 – Division of the time-frequency data into narrow frequency bands of bandwidth  $B$ , reference frequency  $f_i$ , and  $N$  time segments of length  $T_s$  ( $NT_s = T_0$ ). Each time-frequency segment is then analyzed separately, allowing for effective parallelization.

relatively well-determined parameters) are subjected to a final scrutinizing follow-up (a "targeted search").

#### 4 Continuous gravitational waves in the Advanced LIGO O1 era

The first Advanced LIGO observing run (O1) started on September 11, 2015 and finished January 19, 2016. During that time the Hanford and Livingston detectors collected 78 days and 66 days of science data, respectively.

First published result pertains to a targeted search for gravitational waves from 200 known pulsars<sup>17</sup>. In this list, 11 high-value target pulsars, for which the spin-down limit based on Eq. 3 could either be improved or closely approached, were identified. These selected pulsars were analyzed by three, largely independent methods: two time-domain-based methods, Bayesian<sup>18</sup> and  $\mathcal{F}/\mathcal{G}$ -statistic<sup>19</sup>, and the frequency-domain-based 5n-vector method<sup>20,21</sup>. The remaining 189 targets were analyzed using the Bayesian method only. The analysis didn't find significant evidence for a gravitational-wave signal from any of these pulsars, but the most constraining upper limits to date on their gravitational-wave amplitudes and ellipticities were obtained. For eight of the high-value target pulsars, new upper limits give improved bounds over the indirect spin-down limit values. For the Crab pulsar, the 95% confidence upper limit for the gravitational-wave radiation energy is  $2 \times 10^{-3} \dot{E}_{rot}$ , and in case of the Vela pulsar, the upper limit is  $10^{-2} \dot{E}_{rot}$ . The limits on ellipticity correspond to the relative deformation (the "mountain") no greater than  $\simeq 10\text{cm}$  and  $\simeq 50\text{ cm}$  for the Crab and Vela pulsars, respectively. For another 32, values within a factor of 10 of the spin-down limit were found: it is likely that some of these will be reachable in future runs of Advanced LIGO and Advanced Virgo. The smallest upper limit was obtained for PSR J1918-0642:  $h_0 = 1.6 \times 10^{-26}$ . These new results improve on previous limits of Initial LIGO/Virgo by more than a factor of two (see the summary Fig. 1 of<sup>17</sup>, where the comparison with the sensitivity curve, initial detector results and the spin-down limits is presented).

Second publication (in the time of writing available as a preprint) is related to a directed search for gravitational waves from a bright X-ray source Sco X-1<sup>22</sup>. Sco X-1 is the brightest Low Mass X-ray Binary (LMXB, a binary system consisting of a neutron star or a black hole, and a normal star with lower mass) in the Galaxy. The X-ray radiation is produced during accretion; neutron stars in these systems are potential sources of continuous gravitational waves because accretion provides a natural method of building a deformation on the star and powering the gravitational-wave emission. There are however challenges in searching for gravitational waves from this particular source. First, the spin frequency of the neutron star is unknown - the search has to cover a broad range of frequencies, which means it requires much more computing power than a directed search in case of a known pulsar. Most likely the spin frequency is not constant, and not even behaving strictly monotonously, but "wandering" i.e., it changes because of the fluctuations in the amount of accreted matter; frequency is also modulated by the orbital motion of the binary system (the signal power is distributed into sidebands i.e., frequencies higher or lower than the gravitational-wave signal frequency). In order to perform an efficient search in these circumstances, a hidden Markov model (a statistical model in which it is assumed that the system is a Markov process with unobserved states, see<sup>23</sup> and references therein and tutorial<sup>24</sup>) was implemented. The search covered a band of frequencies from 60 Hz to 650 Hz. No detection was claimed from this search, but very sensitive upper limits on the gravitational-wave strain were placed (to quote one example: 95% upper limits  $h_0 = 3 \times 10^{-25}$  at 100 Hz, assuming

circular polarization).

We also report on an all-sky search for periodic gravitational waves using the Advanced LIGO's O1 run<sup>25</sup>, in the frequency band of 20–475 Hz and a frequency time derivative range of  $[-1.0, +0.1] \times 10^{-8}$  Hz/s. Several different data-analysis pipelines took part in this study: the *PowerFlux* (see<sup>26</sup> and references therein), the *FrequencyHough*<sup>27</sup>, the *Skyhough*<sup>28</sup> and the *Time-Domain  $\mathcal{F}$ -stat*<sup>29</sup>. The pipelines employ a variety of algorithmic and parameter choices e.g., they primarily use either the frequency or time domain data, adopt different coherence times used in first-stage data processing (from 1800 s to 6 days), and treat differently the narrow spectral artifacts ("lines"). Outliers that survive all stages of any of the four pipelines are examined

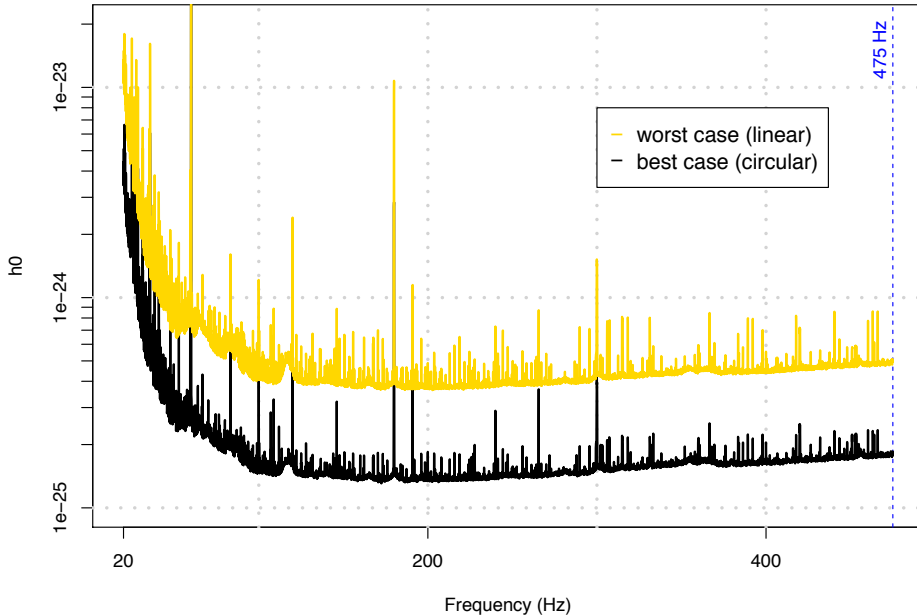


Figure 3 – O1 all-sky upper limits for continuous gravitational waves from the *PowerFlux* pipeline. The upper (yellow) curve shows worst-case (linearly polarized) 95% CL upper limits. The lower (grey) curve shows upper limits assuming a circularly polarized source.

manually for contamination from known, or possibly new, instrumental artifacts. Survivors of this procedure are subjected to additional systematic follow-up used for Einstein@Home searches<sup>30</sup>. Upper limit results are presented in Fig. 3. The lowest upper limits on worst-case (linearly polarized) strain amplitude  $h_0$  are  $\simeq 4 \times 10^{-25}$  near 170 Hz. For a circular polarization (most favorable orientation of the source), the smallest upper limits obtained are  $\simeq 1.5 \times 10^{-25}$ .

In addition, several studies from the Initial Detector Era (LIGO S6 and Virgo VSR2, VSR4 runs) were recently published. They include an all-sky Mock Data Challenge based on the LIGO S6 data<sup>31</sup>, a directed search towards nine supernova remnants<sup>32</sup>, the Orion spur<sup>33</sup>, the globular cluster NGC 6544<sup>34</sup>, as well as the deepest all-sky survey for continuous waves from the Initial Detector Era, the S6 Einstein@Home search in the [50, 505] Hz range<sup>35</sup>. The reason we see merit in publishing the ‘old’ results is to gather experience, test algorithmic improvements and develop new methods using the well-understood data. These new tools are now being used in the O1 (and soon, the O2) searches.

## 5 Plans for the future

The algorithmic and implementation-related improvements acquired during the Dark Ages (2011–2015) will be used to expand the ‘standard’ targeted searches for high-value targets (Sco X-1, Cas A, Vela Jr and G347 supernovae remnants, Crab and Vela pulsars) and to speed up the massive all-sky searches with relatively simple source models (aligned triaxial ellipsoid, Eq. 1). Additionally, we plan to search for signals with more complicated, realistic morphology. The models

include inclined rotating neutron stars, which emit gravitational waves at multiple frequencies at once (e.g., at  $f$  and  $2f$ ), transient continuous gravitational waves emitters (phenomena that may last for weeks to months, and are caused by neutron-star instabilities e.g., the r-modes), and search for non-tensorial gravitational waves. In order to capture the richness of physical processes will be also improving the loosely-coherent methods taking into account the neutron-star frequency wandering, glitches, and a possible mismatch between the gravitational-wave spin frequency parameters and the parameters inferred from the electromagnetic observations.

## Acknowledgments

This work was partially supported by the Polish NCN grant no. UMO-2014/14/M/ST9/00707 and ASPERA/NCN grant 2013/01/ASPERA/ST9/00001.

## References

1. Abbott, B. P., Abbott, R., Abbott, T. D., et al. 2016, *Phys. Rev. Lett.*, 116, 061102
2. Abbott, B. P., Abbott, R., Abbott, T. D., et al. 2016, *Phys. Rev. Lett.*, 116, 241103
3. Aasi, J., Abbott, B. P., et al. 2015, *Class. Quant. Grav.*, 32, 074001
4. Acernese, F., Agathos, M., Agatsuma, K., et al. 2015, *Class. Quant. Grav.*, 32, 024001
5. Andersson, N., & Kokkotas, K. D. 2001, *IJMP D*, 10, 381
6. Lasky, P. D. 2015, *PASA*, 32, e034
7. Einstein, A. 1918 "Sitzungsberichte der Königlich Preussischen Akademie der Wissenschaften zu Berlin", 154
8. Johnson-McDaniel, N. K., & Owen, B. J. 2012, *Phys. Rev. D*, 86, 063006
9. Owen, B. J. 2005, *Phys. Rev. Lett.*, 95, 211101
10. Ushomirsky, G., Cutler, C., & Bildsten, L. 2000, *MNRAS*, 319, 902
11. Wiener, N. 1949, "Extrapolation, Interpolation, and Smoothing of Stationary Time Series", New York: Wiley
12. Helstrom, C. W. 1968, "Statistical Theory of Signal Detection", Pergamon Press, London
13. Schutz, B. F. 1999, *Class. Quant. Grav.*, 16, A131
14. Jaranowski, P., Królak, A., & Schutz, B. F. 1998, *Phys. Rev. D*, 58, 063001
15. Astone, P., et al. 2010, *Phys. Rev. D*, 82, 022005
16. Wette, K. 2014, *Phys. Rev. D*, 90, 122010
17. Abbott, B. P., Abbott, R., Abbott, T. D., et al. 2017, *ApJ*, 839, 12
18. Dupuis, R. J., Woan, G. 2005, *Phys. Rev. D*, 72, 102002
19. Jaranowski, P., Królak, A. 2010, *Class. Quant. Grav.*, 27, 194015
20. Astone, P., DAntonio, S., Frasca, S., Palomba, C. 2010, *Class. Quant. Grav.*, 27, 194016
21. Astone, P., et al., 2012, *JPCS*, 363, 012038
22. Abbott, B. P., et al., 2017, *Phys. Rev. D*, 95, 122003
23. Baum, L.E., 1972, *Inequalities*, 3, 1
24. Rabiner, L. 1989, Proceedings of the IEEE, 77, 257
25. Abbott, B. P., et al. 2017, *Phys. Rev. D*, 96, 062002
26. Aasi, J. et al., 2016, *Phys. Rev. D*, 94, 042002
27. Aasi, J. et al., 2016, *Phys. Rev. D*, 93, 042007
28. Aasi, J. et al., 2014, *Class. Quant. Grav.*, 31, 085014
29. Aasi, J. et al., 2014, *Class. Quant. Grav.*, 31, 165014
30. Papa, M. A., et al., 2016, *Phys. Rev. D*, 94, 122006
31. Walsh, S. et al., 2016, *Phys. Rev. D*, 94, 124010
32. Aasi, J. et al., 2015, *ApJ*, 813, 1
33. Aasi, J. et al., 2016, *Phys. Rev. D*, 93, 042006
34. Abbott, B. P., et al., 2016, *Phys. Rev. D*, 95, 082005
35. Abbott, B. P., et al. 2016, *Phys. Rev. D*, 94, 102002